JCTC Journal of Chemical Theory and Computation

Article

pubs.acs.org/JCTC

Dry Martini, a Coarse-Grained Force Field for Lipid Membrane Simulations with Implicit Solvent

Clément Arnarez,[†] Jaakko J. Uusitalo,[†] Marcelo F. Masman, Helgi I. Ingólfsson, Djurre H. de Jong, Manuel N. Melo, Xavier Periole, Alex H. de Vries, and Siewert J. Marrink*

Groningen Biomolecular Sciences and Biotechnology Institute and Zernike Institute for Advanced Materials, University of Groningen, Nijenborgh 7, 9747 AG Groningen, The Netherlands

Supporting Information

ABSTRACT: Coarse-grained (CG) models allow simulation of larger systems for longer times by decreasing the number of degrees of freedom compared with all-atom models. Here we introduce an implicit-solvent version of the popular CG Martini model, nicknamed "Dry" Martini. To account for the omitted solvent degrees of freedom, the nonbonded interaction matrix underlying the Martini force field was reparametrized. The Dry Martini force field reproduces relatively well a variety of lipid membrane properties such as area per lipid, bilayer thickness, bending modulus, and coexistence of liquid-ordered and disordered domains. Furthermore, we show that the new model can be applied to study membrane fusion and tether formation, with results similar to those of the standard Martini model. Membrane proteins can also be included, but less quantitative results are obtained. The absence of water in Dry Martini leads to a significant speedup for large systems, opening the way to the study of complex multicomponent membranes containing millions of lipids.

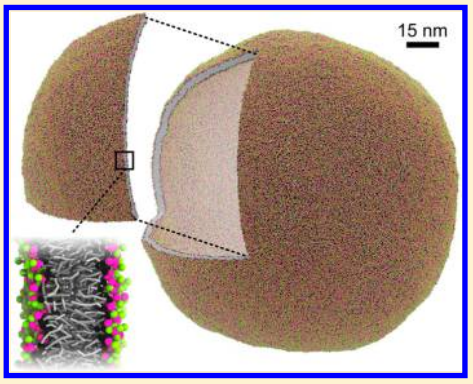

1. INTRODUCTION

Coarse-grained (CG) models have gained a lot of popularity in the field of (bio)molecular simulation. Neglecting some of the atomistic degrees of freedom, CG models allow for a substantial alleviation of both the spatial and temporal limitations of all-atom (AA) models.[1,2] The Martini model is an example of a CG force field that has been widely applied to study a large variety of biomolecular processes, with a focus on cellular membranes.[3] The Martini force field is based on a combined top-down and bottom-up parametrization strategy. Experimental data, in particular thermodynamic data such as partitioning free energies of small organic compounds, are used as main targets for parametrization of the nonbonded interactions, and AA simulations are used to derive effective bonded interactions. Careful calibration of the Martini building blocks has resulted in a versatile CG model that still retains a close link to the underlying chemical structures it represents. Because of the reduced number of degrees of freedom as well as the speedup resulting from the smoothening of the energy landscape and the ability to use larger time steps, the Martini model samples phase space about 3 orders of magnitude faster than AA models.

However, solvent degrees of freedom are computationally expensive, and implicit-solvent models have shown enduring popularity.[4] Even though the Martini force field unites four water molecules in a single CG bead, the explicit solvent can still be a large computational burden. For instance, in a recent Martini application of tether pulling from lipid membranes,[5] some of the systems simulated contained close to 4 million CG beads, of which more than 90% were water, implying that almost all of the considerable computational effort was spent on calculating interactions involving solvent beads. Additionally, Martini water is essentially a Lennard-Jones (LJ) fluid, neglecting explicit hydrogen bonding, dielectric screening, and entropic contributions from individual water molecules. The Martini water model is primarily used to mediate the hydrophobic driving force and to carry hydrodynamic momentum. The shortcoming of implicit screening can be partially alleviated by using a polarizable water model for Martini,[6,7] but a CG water model remains necessarily limited.

Given the simplistic representation of water, one may wonder whether the Martini model could do without explicit water altogether. CG models with implicit solvent are abundant and have been applied to study many aspects of generic membrane behavior.[8−12] Recently, several groups have attempted to incorporate fine chemical detail into such solvent-free models using structure-based coarse-graining. Examples include the models of Voth and co-workers,[13,14] Lyubartsev and co-workers,[15] Wang and Deserno,[16,17] Sodt and Head-Gordon,[18] and Curtis and Hall,[19] all of which use a similar number of CG beads per lipid (10−15) and derive their CG potentials from representative AA simulations. In the pioneering work of the Voth group, force matching between CG and AA systems was used to derive detailed solvent-free models for a number of different lipid mixtures. Lyubartsev and

Received: June 2, 2014
Published: December 2, 2014

co-workers used Newton's inversion method to capture the fine details of the AA model into the CG potentials. Wang and Deserno and Sodt and Head-Gordon added long-range attractive interactions on the lipid tails to mimic the hydrophobic effect, which they tuned to fit experimental data. Curtis and Hall used hard-sphere and square-well potentials in order to use discontinuous molecular dynamics and gain even greater speedup. In a recent model by Srivastava and Voth[20] with three or four beads per lipid, analytical potentials describing the generic behavior of the lipids are combined with detailed force matching potentials that give the model chemical specificity.

Here we aim to provide a solvent-free version of Martini, so-called Dry Martini. The Dry Martini force field is directly based on the standard wet Martini force field and inherits some basic features of wet Martini such as a building-block approach using LJ potentials for the nonbonded interactions between the CG beads. The interaction potentials are therefore more simplistic compared with the potentials obtained through force matching or Newton's inversion underlying the models mentioned above, which implies that our implicit-solvent model is more qualitative in nature. However, a major advantage over existing solvent-free models is the large diversity of molecules already parametrized with the standard Martini model. By recalibration of the interaction matrix of the Martini building blocks, the new model can be directly applied to a variety of processes involving lipid membranes without the need to go through a time-consuming parametrization process based on AA reference simulations. We demonstrate the efficiency of our approach by comparing a variety of membrane properties obtained using standard wet Martini and Dry Martini. These include area per lipid, average tail order parameter, lateral lipid diffusion coefficient, and membrane area compressibility for a large set of lipid types. We also compare the behavior of the explicit and implicit water models in a number of other important membrane processes, such as the formation of raft domains, membrane fusion, and tether formation. Following the historical development of standard Martini, which was initially parametrized for lipids, this version of Dry Martini is aimed at simulation of systems containing principally lipids.

2. METHODS

2.1. Simulation Setup. Simulations were performed with versions 4.5.*x* and 4.6.*x* of the GROMACS package.[21] Time steps of 30 or 40 fs were used to integrate the equations of motion. Simulations with explicit solvent were performed with the velocity-rescaling thermostat of Bussi et al.,[22] unless mentioned otherwise. The time constant of the thermostat was set to $\tau_T = 1.0$ ps. All of the water-free simulations used the second-order stochastic dynamics (SD) integrator in GROMACS with the friction in the Langevin equation set with a time constant of $\tau_t = 4.0$ ps. Unless specifically stated otherwise, the temperature was set to 310 K as the default.

In both wet Martini and Dry Martini, the Berendsen barostat[23] was used to relax the pressure in newly built systems, after which a Parrinello−Rahman barostat[24] was used. All of the bilayer systems were simulated with semi-isotropic pressure coupling. In explicit-water systems, the directions parallel and normal to the bilayer surface were coupled separately to the pressure bath, with a reference pressure of 1 bar. In implicit-water systems, the box was fixed in the direction normal to the bilayer surface by setting the compressibility to 0 bar^{-1}. Furthermore, the membrane was made tensionless by setting the reference pressure in the plane of the bilayer to 0 bar. A value of 3×10^{-4} bar^{-1} was used for the compressibility along the axis of the bilayer plane, with a time constant, τ_p, of 4.0 ps for both force fields. It should be noted that, in general, implicit-solvent simulations should be run in the *NVT* ensemble, as there is no explicit aqueous phase as a reference for the pressure coupling; for periodic planar bilayers, however, a non-null value of the compressibility associated with a semi-isotropic pressure coupling can be used to equilibrate the area per lipid as long as the particle density outside the bilayer is low enough not to contribute significantly to the pressure. Homogeneous systems were simulated using isotropic pressure coupling with a reference pressure of 1 bar, $\tau_p = 4.0$ ps, and a compressibility of 3×10^{-4} bar^{-1}.

The wet Martini and Dry Martini simulations used the same interaction cutoff scheme: van der Waals interactions were smoothly shifted to zero between 0.9 and 1.2 nm, and Coulomb interactions were screened by a relative permittivity constant, ε_r, of 15 and shifted to zero between 0.0 and 1.2 nm. This interaction scheme makes both the potential and the forces vanish at the cutoff.[25] The neighbor list was extended to 1.4 nm and updated every 10 steps.

2.2. Free Energy Calculations. Partitioning free energies were calculated using a free energy perturbation method to decouple the solute from the solvent. The free energy of each transformation was calculated with the Bennett's acceptance ratio (BAR) method[26] as implemented in the *g_bar* GROMACS tool. Intramolecular interactions were not decoupled during the transformations. Each transformation was done with 15 windows, and states were placed twice as densely for λ between 0.30 and 0.70. The soft-core parameters used were sc-α = 0.5, sc-power = 1, and sc-σ = 0.47, and at each λ value the simulation was 100 ns long. The SD integrator was used for both wet Martini and Dry Martini simulations to sample the weakly coupled states properly. The error estimates reported are standard errors obtained by dividing the data into five blocks treated as independent measurements.

2.3. Potential of Mean Force Calculations. The potential of mean force (PMF) as a function of the distance between beads was obtained using umbrella sampling.[27] Umbrella windows were spaced 0.1 nm apart, and each window was simulated for 100 ns using a harmonic restraining potential on the distance with a force constant of 1000 kJ mol^{-1} nm^{-2}. The separate distributions were combined using the weighted histogram analysis method[28] as implemented in the GROMACS program *g_wham*.[29] Bayesian bootstrapping of complete histograms was used to generate 200 PMFs, the standard deviation of which gave an estimate of the error of the PMF.

2.4. Calculation of Bilayer Properties. The bilayer density profiles were calculated using the *g_density* tool in GROMACS. The bilayer thickness, l_{PO4}, was taken as the distance between the density maxima of the PO4 beads (phosphate groups) of the lipids in the two leaflets. The area per lipid, A_l, was calculated as the average box area during the simulation divided by the number of lipids in each leaflet. The lipid tail segmental order parameter, S_{seg}, was calculated from the angle θ between the normal of the bilayer surface and the vector along each bond in the lipid tails as follows:

$$S_{seg} = \frac{1}{2}(3\langle\cos^2\theta\rangle - 1) \quad (1)$$

The bilayer area compressibility, K_A, was calculated from the amplitude of the box area fluctuations as described in ref 30:

$$K_A = k_B T \frac{\langle A \rangle}{N \langle (A - A_0)^2 \rangle} \quad (2)$$

where k_B is the Boltzmann constant, T is the absolute temperature, N is the number of lipids in each leaflet, and A_0 is the average projected area. The reported errors are standard errors obtained from block averaging: the number of blocks was varied from 1 to a value high enough that each block had only five data points, and the reported error is the maximum standard error found within the last 20% of the block sizes studied.

The lateral diffusion of lipids was extracted from the mean square displacement (MSD) of the PO4 beads obtained with the *g_msd* tool in GROMACS. The center-of-mass motion of the system was first removed, and the diffusion coefficient of the lipids, D, was obtained by fitting the MSD curve versus time (omitting 10% of the data at both ends) to the linear regression $\mathrm{MSD}(t) = 4Dt + C$, where the constant C takes care of the offset at $t = 0$. The reported error is the difference between the fits to the first and second halves of the MSD curve as done by *g_msd*.

The lateral pressure profiles were determined using a modified version of the GROMACS package version 4.0.2, available at ftp://ftp.gromacs.org/pub/tmp/, following a formalism described previously.[31] Briefly, the lateral pressure, $p(z)$, may be obtained as the difference between the lateral component, P_L, and the normal component, P_N, of the pressure tensor, that is, $P_L = (P_{xx} + P_{yy})/2$ and $P_N = P_{zz}$. In practice, the system was first divided into a 3D grid with a cell size of 0.3 nm. The local pressure tensor was then analyzed for each grid point, and averages were calculated over the xy plane along the normal of the bilayer (z axis).

The membrane bending modulus, κ, was calculated from the undulation spectrum $S_u(q)$ of a large lipid patch using the method described by Brandt et al.[32] A wave vector bin spacing of 0.1 nm^{-1} was used. The low-q regime of the spectrum was fitted to

$$S_u(q) = \frac{k_B T}{A_l \kappa q^4} \quad (3)$$

where A_l is the area per lipid and q is the wave vector. An error estimate of the bending modulus was obtained from the sensitivity of the fit to the number of data points included.

2.5. Construction of Planar Bilayers and Giant Vesicles. The planar bilayer systems were set up using the *insane.py* script, which builds a bilayer structure from template lipids and minimizes conflicting overlaps so that a minimization is sufficient to obtain a conformation ready for equilibration. The initial bilayer structures were equilibrated in two steps, a short 0.5 ns simulation with a small time step (10 fs) followed by a 30 ns simulation with the regular time step (30 fs) and using the Berendsen barostat[23] to equilibrate the box dimensions. From this starting protocol, several different membrane systems were simulated, as detailed in the Results.

The vesicles were created with another in-house script, *vesicle-builder.py*, which builds arbitrarily sized vesicles with arbitrary lipid composition in each leaflet. By approximating a vesicle with a polyhedron (each leaflet independently), the program orients and places lipids on a grid formed by each vertex in such a way that the planar lipid bilayer properties (area per lipid, bilayer thickness, and/or a weighted average in the case of lipid mixtures) are respected. The deviations from these properties due to the curvature of the vesicles needed careful relaxation before any production runs. Both scripts are available for download from the Martini portal (http://cgmartini.nl/).

3. RESULTS

Our aim was to build an implicit-water Martini ("Dry Martini") force field for lipids that, while being much faster, would reproduce the behavior of standard Martini as closely as possible. Thus, the most appropriate benchmark to test how well it performs is a direct comparison to results obtained using the standard "wet" Martini force field. After introducing the parameters of Dry Martini in section 3.1, in section 3.2 we compare the partitioning behavior of individual CG beads in wet Martini and Dry Martini. In section 3.3 the dimerization of CG beads in different solvents is investigated. Standard properties of lipid bilayers and details of their phase behavior are described in sections 3.4 and 3.5, respectively. In section 3.6 we present a set of large-scale applications. Issues related to the behavior of proteins in Dry Martini are presented in section 3.7.

3.1. Dry Martini Force Field Parameters. The Martini model differentiates between four main types of particle: polar (P), nonpolar (N), apolar (C), and charged (Q). Within each type, subtypes are distinguished either by a letter denoting the hydrogen-bonding capabilities (d for donor, a for acceptor, da for both, and 0 for none) or by a number indicating the degree of polarity (from 1 for low polarity to 5 for high polarity), giving a total of 18 particle types. In Dry Martini, the same bead types as in standard Martini are used, assuring maximum transferability between the models. Nonbonded interactions between these particle types are described by a shifted LJ 12−6 potential. The standard particle size parameter, σ, is 0.47 nm for all particle types except for the class of ring particles, for which σ equals 0.43 nm. The strength of the interaction, determined by the value of the LJ well depth, ε, depends on the interacting particle types and is given by a limited number of levels tabulated in the Martini interaction matrix.[30,33]

In standard Martini, the hydrophobic effect is modeled by having stronger pairwise interactions between similar polar (P-type) and apolar (C-type) bead types compared with their cross interactions. In Dry Martini, the removal of the aqueous phase has to be somehow compensated with other interactions in the force field. Instead of introducing a specific term to account for solvation effects, we chose to adjust the strength of existing pairwise LJ interactions to retain the hydrophobic/hydrophilic behavior of molecules in standard Martini. The adjustment of the LJ interactions followed an iterative trial-and-error procedure in which the effects of changes in the interaction matrix were tested on the systems described in sections 3.2−3.7 by comparison with standard Martini. Starting from an intuitive initial guess of which interactions should be weakened or strengthened to mimic the absence of solvent, a more systematic approach was followed. The LJ interactions of charged (Q-type) particles were first explored through comparison of ion−ion interactions in implicit and explicit solvent. These parameters were then transferred to lipid headgroups and further optimized by comparing the thickness and area per lipid of bilayers to the results from standard Martini. This scan was then extended to the interactions involving the glycerol linker and finally the tails. Concurrently, we calculated the partitioning free energies of each bead type from ether, chloroform, hexadecane, and octanol to water and compared the values to those obtained with standard Martini.

Table 1. Nonbonded Interaction Table for Dry Martini[a]

	Qda	Qd	Qa	Q0	P5	P4	P3	P2	P1	Nda	Nd	Na	N0	C5	C4	C3	C2	C1
Qda	VI																	
Qd	VI	VII																
Qa	VI	VI	VII															
Q0	VIII	VIII	VIII	VIII														
P5	XII	XII	XII	XII	V													
P4	XII	XII	XII	XII	V	VI												
P3	XII	XII	XII	XII	V	VI	VI											
P2	XII	XII	XII	XII	V	VII	VII	VII										
P1	XII	XII	XII	XII	X	X	X	VIII	VII									
Nda	XII	XII	XII	XII	XII	XI	XI	XI	VII	VI								
Nd	XII	XII	XII	XII	XII	XI	XI	XI	VII	VI	VII							
Na	XII	XII	XII	XII	XII	XI	XI	XI	VII	VI	VI	VII						
N0	XII	XII	XII	XII	XII	XI	X	IX	VII	VII	VII	VII	V					
C5	XII	XII	XII	XII	XII	XI	X	VI	VI	VI	VI	VI	V	III				
C4	XII	XII	XII	XII	XII	XI	X	VI	VI	VI	VI	VI	IV	III	II			
C3	XII	XII	XII	XII	XII	XI	X	VII	VI	VI	VI	VI	IV	III	II	II		
C2	IX	IX	IX	IX	XII	XII	X	VIII	VI	VI	VI	VI	IV	III	III	II	II	
C1	IX	IX	IX	IX	XII	XII	XI	X	VII	VI	VI	VI	IV	III	III	II	II	II

[a]The interaction level dictates the strength of the Lennard-Jones potential between two bead types. Only the ε parameter changes according to the interaction level. From the strongest to the weakest interaction, the levels have the following interaction strengths (in kJ mol^{-1}): ε_0 = 5.6, ε_I = 5.0, ε_{II} = 4.5, ε_{III} = 4.0, ε_{IV} = 3.5, ε_V = 3.1, ε_{VI} = 2.7, ε_{VII} = 2.3, ε_{VIII} = 2.0, ε_{IX} = 2.0, ε_X = 1.5, ε_{XI} = 1.0, ε_{XII} = 0.5. Dry Martini only uses interaction levels II–XII, but the naming convention was kept the same as in standard Martini, e.g., level V of standard Martini has the same interaction strength as level V of Dry Martini. Most beads use the standard Martini interaction distance σ = 0.47 nm. However, Q–Q interactions use σ = 0.60 nm. The interaction distance for level IX was kept at σ = 0.62 nm as in standard Martini for both regular and S-type particles. Also see Figure S1 in the Supporting Information for a comparison between the interaction matrices of standard Martini and Dry Martini.

Bilayer simulations were used to reject LJ parameters that reproduced the partitioning properties but impacted the bilayer properties (e.g., overestimated ordering of the lipid tails because of too-strong attraction).

The resulting interaction matrix for Dry Martini is presented in Table 1, and the matrix for standard Martini is shown for comparison in Figure S1 in the Supporting Information. The original interaction levels of standard Martini are kept, although the strongest levels (0 and I) are not used in Dry Martini. We found that the strength of interactions between polar beads had to be significantly decreased to mimic the hydration effect. The description of the self-interactions between polar beads therefore required the addition of three new interaction levels, X–XII, with relatively weak interaction strengths: ε_X = 1.5 kJ mol^{-1}, ε_{XI} = 1.0 kJ mol^{-1}, and ε_{XII} = 0.5 kJ mol^{-1}. In contrast, the interaction between apolar beads was strengthened to retain the hydrophobic effect as modeled in standard Martini. The treatment of ring particles in standard Martini, which are modeled with smaller (S-type) beads, was kept in Dry Martini: σ is reduced to 0.43 nm, and ε to 75% of their normal values. The lack of implicit solvent also led to the need to readjust the charge–charge interactions. Charged (Q-type) beads are considered fully hydrated in Dry Martini. The Q-type self-interactions are therefore modeled with an increased σ of 0.60 nm. The screening of the Coulombic interactions is performed using a relative dielectric constant ε_r = 15, the same as in standard Martini. Together with the shifting function applied on the potential, this results in an effective distance-dependent screening that reaches infinity at the cutoff distance of 1.2 nm.

Modifications of the nonbonded interactions may affect structural parameters, which can be compensated by adjusting bonded parameters. For example, the increase in the interaction strength between apolar beads led to the need for an adjustment of the bonded parameters in the lipid tails to keep the same equilibrium bond lengths. Specifically, the reference distance for the bond between the headgroup beads was shortened from 0.47 to 0.45 nm, while the bonds between the tail beads was increased from 0.47 to 0.48 nm. The angle potentials in the lipid tails were also slightly adjusted to better reproduce bilayer thicknesses and lipid order parameters: the best fit was achieved by making saturated tails stiffer with an angle force constant of 35.0 kJ mol^{-1} (vs 25.0 kJ mol^{-1} in standard Martini) and changing the angle parameters for polyunsaturated tails to a reference angle of 95.0° and a 20.0 kJ mol^{-1} force constant (vs 100.0° and 10.0 kJ mol^{-1}, respectively, in standard Martini). Examples of representative bond and angle distributions are given in Figure S2 in the Supporting Information. Together these changes allow Dry Martini to reproduce both the standard Martini bond length and angle distributions as well as the thickness, area per lipid, and order parameters of standard Martini lipid bilayers, as detailed below. The LJ interaction matrix and lipid topologies for Dry Martini are available at http://cgmartini.nl/.

3.2. Partitioning Free Energies. The partitioning of building blocks (beads) between polar and apolar solvents was a primary parametrization target for standard Martini.[30] Comparison of the partitioning behaviors of wet Martini and Dry Martini is thus an important test. The properties of pure-solvent models naturally will greatly influence the partitioning of the solutes. Despite the drastic changes in the interaction matrix in going from wet Martini to Dry Martini, the densities of other solvents generally used for parametrization (hexadecane, chloroform, ether, and octanol) are reasonably well conserved in Dry Martini. Average densities obtained from 100 ns long simulations of systems containing 100 or 400 solvent molecules (solvents modeled by four beads and one bead, respectively) are given in Table 2 for both Martini versions. Note that the particle types used to represent the solvents remain unchanged between wet and dry Martini: four C1 particles for hexadecane, C4 for chloroform, N0 for ether, and

dx.doi.org/10.1021/ct500477k | J. Chem. Theory Comput. 2015, 11, 260–275

Table 2. Densities of Solvents[a]

solvent	exp	wet	dry
hexadecane	773	659	694
chloroform	1483	1422	1591
ether	714	883	798
octanol	827	879	803

[a]The experimental (exp) densities are reported together with values from wet Martini and Dry Martini. All of the densities are reported in kg m^{-3}. The simulation data were obtained at 310 K, and the experimental values were measured at 293 K.[54] See Methods for simulation details.

C1−P1 for octanol. The bonded interactions for aliphatic solvents (e.g., hexadecane), however, were adjusted in line with the changes in the bonded parameters for the lipids.

Although partitioning free energies can be obtained from equilibrium distributions of solutes in two-phase systems (vacuum/solvent in the case of Dry Martini), the method based on a thermodynamic cycle was used since it is more convenient and more accurate. For Dry Martini, the free energy of decoupling the solute from the solvent equals the partitioning free energy between that solvent and the implicit water phase. We used dodecahedral simulation boxes containing 198 solvent molecules for single-bead solvents (water, chloroform, and ether), 96 molecules in the case of octanol, and 69 molecules in the case of hexadecane. The minimal distance between solute molecules in these boxes was between 3.2 and 3.5 nm. The details of how the solute transformation was performed are presented in section 2.2. The resulting partitioning free energies of standard Martini and Dry Martini as well as experimental values are listed in Table 3. The correspondence between wet Martini and Dry Martini is rather good. The average unsigned deviation of the free energies is 2.9 kJ mol^{-1}, and the median is 2.0 kJ mol^{-1}. The largest discrepancies are found in the case of partitioning of charged (Q-type) particles between water and either ether or octanol. With the current range of interaction levels (cf. Table 1), we are unable to further optimize these partitioning free energies. However, because of the lack of experimental data for charged building blocks, it is difficult to assess how unrealistic Dry Martini is in these cases.

3.3. Bead−Bead PMFs and Ion RDFs. To further examine the correspondence between standard Martini and Dry Martini, potentials of mean force between all possible pairs of bead types were computed both in water and in hexadecane (see section 2.3 for details). To accomplish this, the simulated systems consisted of 400 water or 100 hexadecane molecules in which the two solute beads were embedded. Examples of the resulting PMFs are shown in Figure 1, and the full set is available on request. It should be noted that the PMF between two beads in Dry Martini (implicit water) is equal to the nonbonded interaction potential between those beads. The set of interactions shown in Figure 1 covers the main types of interactions encountered in the Martini force field, namely, nonpolar (N-type, Figure 1A), apolar (C-type, Figure 1B), polar (P-type, Figure 1C), and charged (Q-type, Figure 1D). In all cases, the PMFs indicate comparable interaction strengths in wet Martini and Dry Martini. The most notable difference is the loss of water-mediated structure in Dry Martini. In the case of charge−charge interactions, the increase in the bead size (σ = 0.60 nm) to mimic the hydrated character of the beads results in a shift of the minimum to larger distances.

Table 3. Partitioning Free Energies between Different Solvents[a]

	$\Delta G_{H\to W}$			$\Delta G_{C\to W}$			$\Delta G_{E\to W}$			$\Delta G_{O\to W}$		
	exp	wet	dry	exp	wet	dry	exp	wet	dry	exp	wet	dry
Qda		−56	−52		−21	−18		−14	−8		−22	−9
Qd		−56	−52		−21	−18		−14	−8		−15	−9
Qa		−56	−52		−21	−18		−14	−8		−15	−9
Q0		−56	−52		−21	−18		−13	−8		−15	−9
P5	−27	−31	−24	(−20)	−20	−18	−15	−14	−8	−8	−9	−7
P4	−25	−24	−24		−14	−16	−10	−7	−6	−8	−9	−7
P3	−21/−19	−22	−22	−9	−11	−12	−2	−8	−3	−5/−1	−9	−6
P2	−13	−17	−17	−5	−3	−2	−3	1	−3	−2	−4	−2
P1	−10/−9	−13	−11	−2	−3	−2	−1/0	1	3	0/1	−2	2
Nda	−5	−9	−6	2	−2	−2	4	1	3	4	2	3
Nd	(−6)	−9	−6	(1)	−2	−2	(−3)	1	3	(3)	2	3
Na	−6/−5/−4	−9	−6	1/(4)	−2	−2	(−1)/2	1	3	−2/−1/3	2	3
N0	1	−4	2		6	5	(3)	6	9	(3)	4	7
C5	(7)	3	8		9	10		9	9	(9)	7	11
C4	11/(7)	7	13	14	13	15		13	12	9/11	10	13
C3	12	11	13		13	15		13	12	12/13	12	13
C2		14	13		13	15		13	12	14	14	13
C1	18	16	13		15	15		12	12	16	14	12

[a]The reported partitioning free energies (in kJ mol^{-1}) are the free energies of moving the solute from the other solvent to water. W denotes water, H hexadecane, C chloroform, E ether, and O octanol. The statistical error in each partitioning free energy is less than 0.3 kJ mol^{-1}; however, all of the values are rounded to integers as the accuracy of the force field is considered to be at most 1 kJ mol^{-1}. All of the simulation data were obtained at 310 K. Experimental values are from refs 55−60 and were collected at temperatures between 298 and 300 K. Parentheses around an experimental value denote that the value was obtained from the result for a similar compound. A list of values is given when the bead type in Martini has more than one model compound. The wet Martini values were recalculated using a procedure identical to that for the Dry Martini values. The differences between the values reported here and in the original publication[33] are due to the improved sampling and the fact that these simulations are infinitely dilute. In the case of octanol, the values given here pertain to dry octanol.

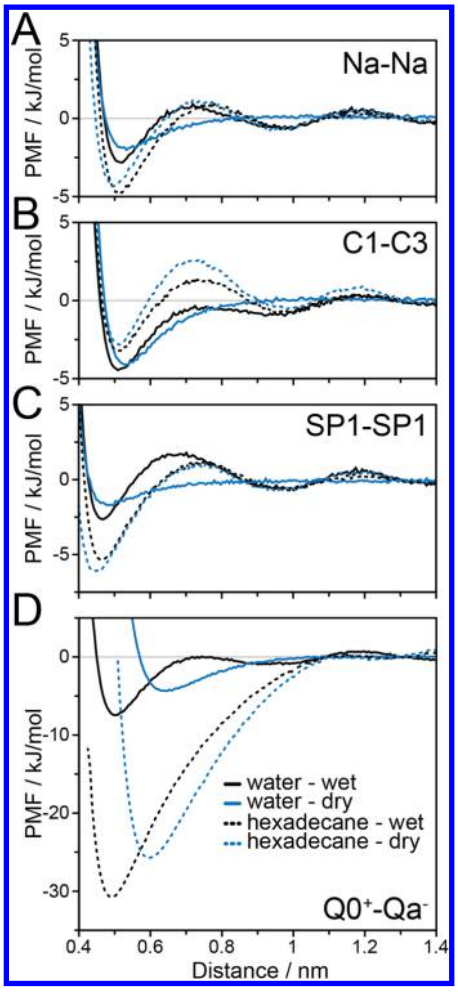

Figure 1. Comparison of four bead−bead potentials of mean force (PMFs) in wet Martini and Dry Martini. (A) Na−Na, e.g., modeling interactions between glycerol linkers in the Martini lipids. (B) C1−C3, representative of tail−tail interactions. (C) SP1−SP1, e.g., modeling the interaction between cholesterol sites. (D) $Q0^+-Qa^-$, e.g., modeling the interaction between choline and phosphate beads of PC lipids.

In view of the substantial differences observed for the effective interactions between charged bead pairs, it was of interest to analyze the behavior of ionic solutions. To this end, we simulated systems containing 200 Na^+ and 200 Cl^- ions in a box with a volume of 682 nm^3, which corresponds to an ion concentration of ∼500 mM. Simulations with Dry Martini were performed at constant volume (*NVT*). Standard Martini simulations were run in an *NpT* ensemble and contained 5300 explicit Martini water beads. The simulations were 1.6 μs long, from which the first 10 ns were discarded as equilibration. In Figure 2 we present the results of these simulations in the form of radial distribution functions (RDFs) between the various ion pairs. The Na^+-Cl^- RDFs from the explicit- and implicit-solvent simulations differ considerably (Figure 2A). The first peak is lower, broader, and located at a larger distance in Dry Martini, reflecting the implicit description of full hydration, while standard Martini models ions as partially hydrated. The inclusion of full hydration in the Dry Martini charged particles was designed to describe the hydrated character of charged lipid headgroups. In turn, this feature prevents tight binding of ions. The overall loss of structure beyond the first neighbor shell directly reflects the lack of

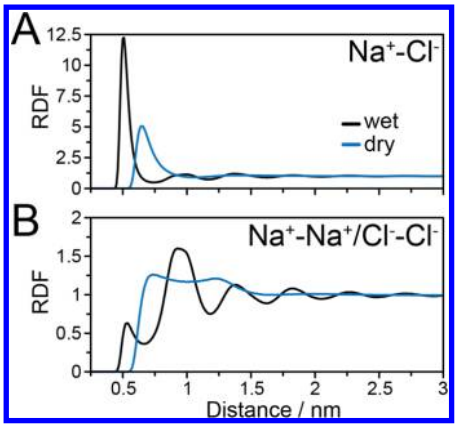

Figure 2. Radial distribution functions (RDFs) of ∼500 mM NaCl solutions in wet Martini and Dry Martini. The RDFs between ions with (A) like and (B) unlike charges are shown separately.

solvation. The RDFs of like-charge ion pairs (Na^+-Na^+ and $Cl^-−Cl^-$) show similar deviations between wet Martini and Dry Martini (Figure 2B). The first-neighbor peak is found at a larger distance and long-range structure is lost in Dry Martini. A broad second-neighbor peak is present, with a significant overlap with the first-neighbor peak; it is due to bridging of the ions with like charge by an ion with unlike charge.

3.4. General Bilayer Properties. The hallmark of the parametrization of Dry Martini was a realistic description of lipid bilayers, making their properties the strong focus of the design of the force field. In section 3.1 we described the modifications of the nonbonded interactions and the associated fine-tuning of the bonded parameters needed to reproduce lipid bilayer properties obtained using the standard Martini model. Here we describe the extent to which the final set of lipid parameters for Dry Martini reproduces bilayer properties of the standard version.

We first focus on the behavior of the ubiquitous bilayer-forming lipid palmitoyloleoylphosphatidylcholine (POPC). Dry Martini POPC lipids self-assemble into bilayers, as shown in Figure 3A for a system containing 504 POPC lipids. The self-assembly process is similar to that observed in AA and standard Martini simulations as reported in ref 34: starting from a randomly dispersed lipid solution (snapshot at t = 0 ns), a rapid local clustering of lipid tails results in a dense mesh of tubular aggregates that quickly relaxes to a bilayer structure; this initial bilayer still contains defects in the form of pores (t = 50 ns), which eventually seal, leaving an intact membrane (t = 100 ns).

The structural and dynamical properties of the equilibrated self-assembled POPC bilayer in Dry Martini are compared to their standard Martini equivalents in Figure 3B,C. The density profiles along the bilayer normal (Figure 3B) show that the distributions of both lipid headgroups and tails are similar in the two models. A slightly more pronounced density dip in the core of the membrane can be noticed for standard Martini. Other properties (area per lipid, bilayer thickness, area compressibility, and average tail order parameter) also compare well between the two models (Figure 3C). The values for these bilayer properties fit well within the range of observed experimental values (Figure 3C). Because of the CG modular building block nature of Martini, both the wet and dry POPC bilayers are thicker than the experimental values. Martini lipids are not optimized to represent specific atomistic lipid types but rather are constructed from a general set of beads and bonded

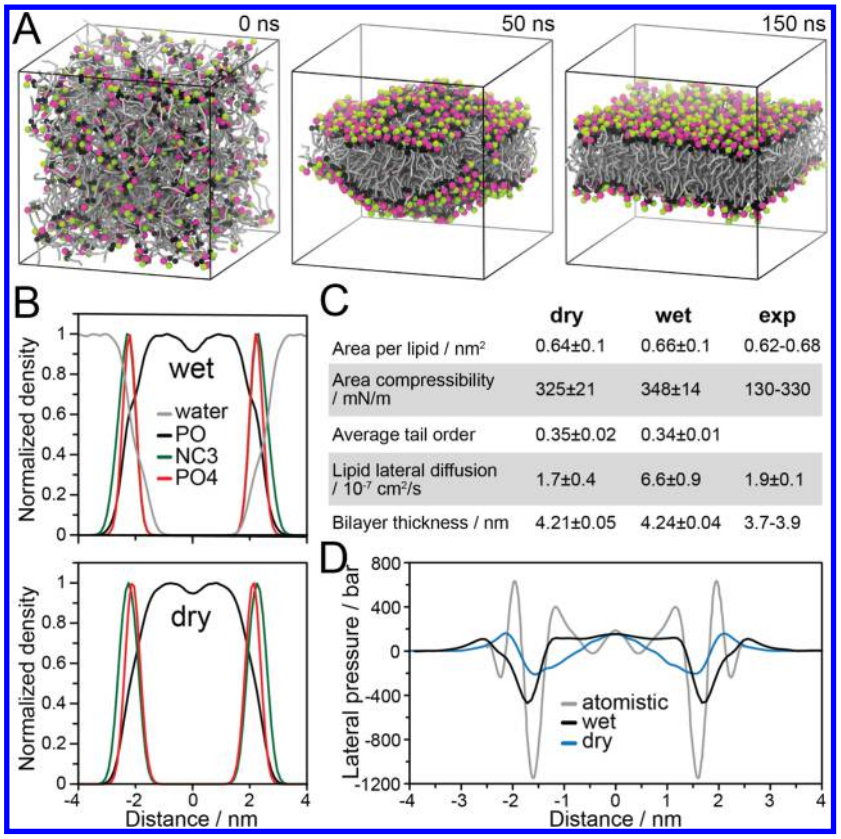

Figure 3. Properties of a POPC bilayer in Dry Martini (dry) compared to wet Martini (wet) and experimental data (exp). (A) Snapshots taken from a simulation of the self-assembly of a bilayer from a set of randomly oriented lipids. (B) Normalized densities of the various moieties (phosphatidyl, PO4; choline, NC3; lipid tails, PO) composing POPC lipids along the bilayer normal (the origin defines the center of the bilayer). Results from both the wet and dry models are reported. (C) Comparison of various structural and dynamical properties. The experimental values were measured between 297 and 323 K and taken from area per lipid,[61−64] area compressibility,[65] lipid diffusion,[66] and bilayer thickness.[63,64] (D) Lateral pressure profiles for an AA model,[35] wet Martini, and Dry Martini.

potentials. As each CG tail bead represents about four carbon atoms, CG POPC, whose longer tail has 5 beads, is somewhat too thick compared to POPC's 18-carbon oleoyl tail. The lipid lateral diffusion rate is an exception: it is decreased by roughly a factor of 3 in Dry Martini. The reason for this difference in lateral mobility is the warranted use of a stochastic integrator in the absence of solvent, introducing friction into the equations of motion (see section 2.1 and Table S2 in the Supporting Information).

As a final test for POPC bilayers, we computed the lateral pressure profile for a system containing 64 POPC lipid molecules in each leaflet and simulated with both wet Martini and Dry Martini. The two profiles are shown in Figure 3D, together with one obtained using the same method but from a simulation of a model at atomistic resolution.[35] In both versions of Martini the pressure profiles are smoother than at the AA level, but the overall features of the profile, e.g., negative pressure in the headgroup regions and positive pressure in the tail region, are preserved. The pressure profiles of standard Martini and Dry Martini are similar.

For a more detailed view of the structural organization of lipid bilayers, we studied the lateral organization of PC headgroups. We compared RDFs computed between phosphate moieties extracted from simulations of dipalmitoylphosphatidylcholine (DPPC) using different force fields (wet Martini, Dry Martini, AMBER-GAFF, and Gromos 54a7). The results are reported in Figure 4. Compared with standard Martini, the first peak in the RDF is shifted toward increased

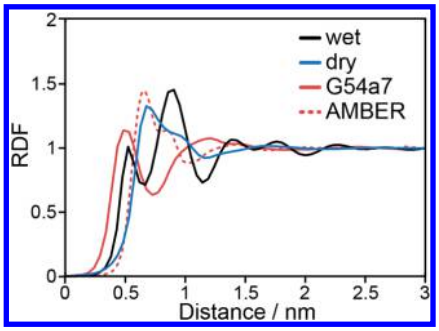

Figure 4. Phosphate−phosphate RDFs describing DPPC structures obtained with various force fields. All of the explicit-solvent simulations were carried out at T = 323 K and Dry Martini simulations at 330 K to avoid the DPPC gel phase. A common setup for Gromos 54a7 and AMBER-GAFF simulations was used.

distances in Dry Martini. This difference can be attributed to the larger bead sizes of the Q particles in our dry model, taking into account an implicit solvation shell. Thus, the lateral organization of the lipid headgroups is dissimilar in wet Martini and Dry Martini, despite the similarity in global bilayers properties described above. Comparing the RDFs of the Martini models to the results obtained with the atomistic force fields gives rise to an interesting observation. Whereas the RDF obtained with standard Martini most closely resembles that of Gromos 54a7, the Dry Martini result is actually much closer to the RDF obtained with AMBER-GAFF. Apparently the lateral

dx.doi.org/10.1021/ct500477k | J. Chem. Theory Comput. 2015, 11, 260−275

organization of the lipid headgroups is very sensitive to details of the force field. As we have no means of assessing which of the two atomistic force fields is more realistic here, we did not optimize the Dry Martini model further on the basis of these RDFs.

To extend our comparison of bilayer properties to other lipids, we created a large set of preformed lipid bilayers combining four different phosphate headgroups (phosphatidylcholine, PC; phosphatidylethanolamine, PE; phosphatidylglycerol, PG; and phosphatidylserine, PS) with 18 different lipid tails. The tail length was varied from two to six CG beads (representing atomistic tails from 8 to 26 carbons), and the level of saturation in the tail was varied from fully unsaturated to fully saturated. Together this set of lipids covers a large variety of biologically relevant lipid species (see Table S2 in the Supporting Information for a list of all of the lipid types used). Each system was composed of 242 lipids and simulated for 1 μs using the dry model. Reference simulations using standard Martini were performed under the same conditions at the full hydration level (>11 CG water beads or 44 water molecules per lipid). In each case, the last 0.9 μs were used for analysis of the area per lipid, bilayer thickness, average tail order parameter, lateral lipid diffusion coefficient, and membrane area compressibility. Correlation plots of Dry Martini versus wet Martini for the area per lipid and bilayer thickness are given in Figure 5. The results for the remaining properties can be found in Figure S3 in the Supporting Information. Additionally, Table S2 lists all of the properties for all of the lipid types.

Overall, Dry Martini bilayers behave similarly to the respective wet versions. Linear fits of the data give slopes of 0.81 and 1.24 with R^2 values of 0.90 and 0.92 for the area per lipid and bilayer thickness, respectively. In both cases there is a high correlation between wet Martini and Dry Martini. However, the deviation of the slopes from unity indicates that in Dry Martini the bilayers of short lipids are slightly too thin and the tails spread out, whereas bilayers of long lipids are slightly too thick and densely packed. As a direct consequence, Dry Martini lipids tend to go into the gel phase at lower temperatures than in wet Martini (see section 3.5), following more closely the experimental behavior. Lipids in different phases in wet Martini or Dry Martini were excluded from the comparisons of bilayer properties above.

Another property of interest is the bending rigidity of the membrane. To compare the bending rigidities of wet Martini and Dry Martini lipids, a bilayer patch of 8192 dimyristoylphosphatidylcholine (DMPC) lipids was simulated for 2.5 μs. This simulation was used to calculate the undulation spectrum (Figure S4 in the Supporting Information) as described in Methods, discarding the first 500 ns as an equilibration period. From the low-q range of this spectrum, the bending modulus κ was obtained (see Methods). For standard Martini, we obtained $\kappa = (14 \pm 1) \times 10^{-20}$ J, which is comparable to recently published values for standard Martini ($(15-17) \times 10^{-20}$ J).[32,36] The bending modulus obtained for dry DMPC lipids, $\kappa = (11 \pm 1) \times 10^{-20}$ J, is on the same order, albeit somewhat smaller. For comparison, a bending modulus of $\kappa = 8 \times 10^{-20}$ J was found for an AA simulation,[32] and the range of experimental values reported for DMPC is $\kappa = (5-15) \times 10^{-20}$ J.[37] We conclude that the bending stiffness of the dry Martini model compares reasonably well to the existing literature data.

3.5. Lipid Phase Behavior. To test the Dry Martini model in more complex membrane environments, we simulated

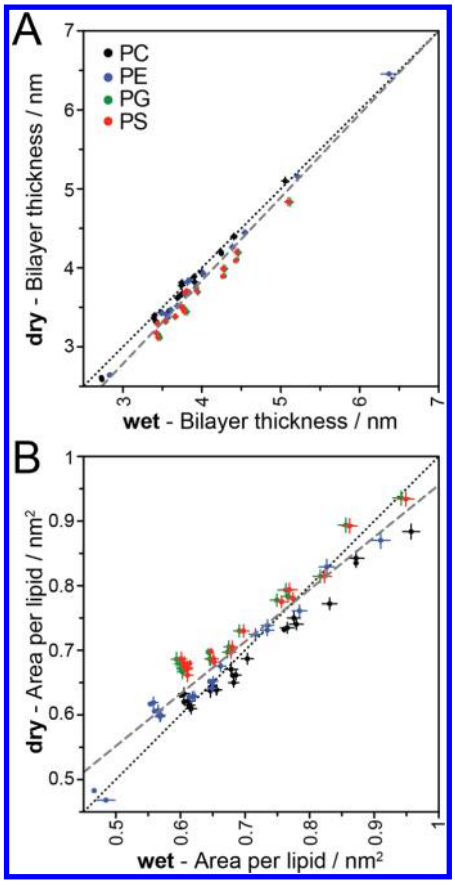

Figure 5. Correlation plots of lipid properties from wet Martini and Dry Martini for 72 different phospholipid species: (A) bilayer thickness; (B) area per lipid. In each panel, the dotted black line marks equality, and the dashed gray line shows a linear fit to the data (excluding lipids that go into the gel phase in Dry Martini). Lipids with different headgroups are color-coded: phosphatidylcholine (PC, black), phosphatidylethanolamine (PE, blue), phosphatidylglycerol (PG, green), and phosphatidylserine (PS, red). A list of the properties for all of the simulations can be found in Table S2 in the Supporting Information.

ternary mixtures of cholesterol (which includes ring particles), saturated (DPPC), and either unsaturated (dioleoylphosphatidylcholine, DOPC) or polyunsaturated (dilineoylphosphatidylcholine, DLiPC) lipids. There is a composition range for which these ternary mixtures are known to undergo phase separation into liquid-ordered (L_o) and liquid-disordered (L_d) domains both experimentally[38] and in standard Martini.[39] We simulated bilayers containing 2000 lipids with a DPPC:DLiPC:cholesterol or DPPC:DOPC:cholesterol ratio of 42:28:30 for a minimum of 5 μs starting from a randomized lateral lipid distribution. Both systems were simulated below the DPPC gel-to-fluid transition temperature. The final configurations from these simulations are shown in Figure 6A. The DPPC/DLiPC/cholesterol system undergoes phase separation into a distinct L_d phase enriched in the unsaturated lipid and an L_o phase composed of mostly DPPC and cholesterol, in good agreement with results obtained with standard Martini.[39] In agreement with experimental results, the DOPC-containing system is also phase-separated into L_d and L_o phases.[38]

The phase-modulating effect of cholesterol was further probed by simulating the same DPPC:DOPC and DPPC:DLiPC proportions in the absence of cholesterol

dx.doi.org/10.1021/ct500477k | J. Chem. Theory Comput. 2015, 11, 260−275

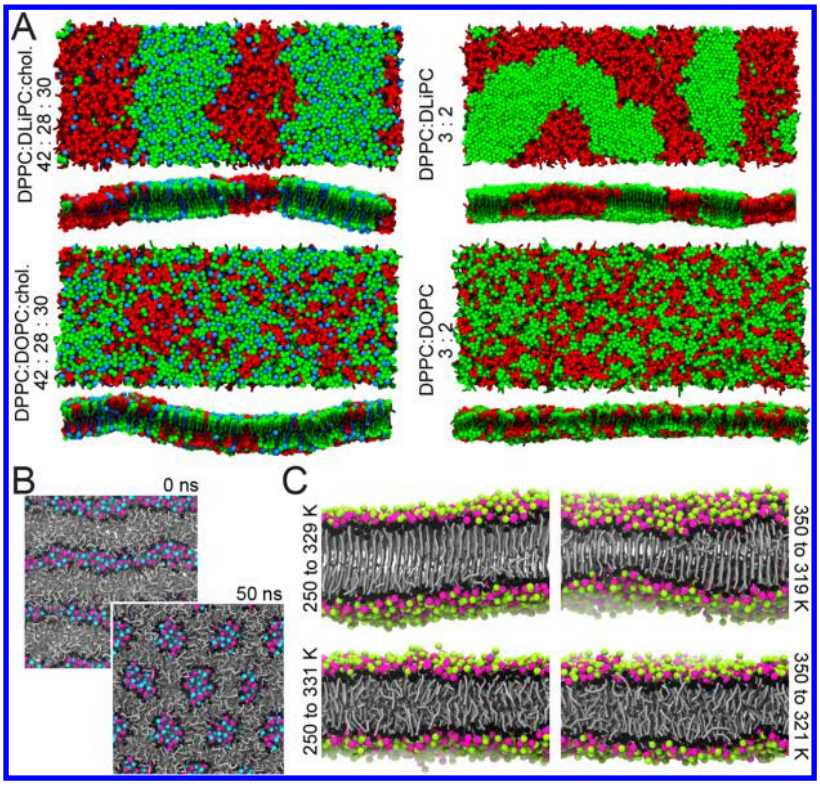

Figure 6. Lipid phase behavior with Dry Martini. (A) Top and side views of planar ternary or binary mixture bilayers after simulations of at least 5 μs. The bilayers are composed of cholesterol (blue), DPPC (green), and either DLiPC or DOPC (red); the binary mixtures have the same proportions of DPPC and DLiPC/DOPC but no cholesterol. The lipid headgroups have been omitted for clarity, and the two first tail beads of each lipid tail as well as the bead containing the cholesterol OH group are highlighted as spheres. The side views highlight the tail ordering in the DPPC-enriched domains, even in the less visibly phase-separated DPPC/DOPC/cholesterol system. (B) Transition from multilamellar to inverted hexagonal phase of a pure eicosapentaenoylphosphatidylethanolamine system. Phosphatidyl and ethanolamine moieties, the glycerol backbone, and the aliphatic section of the lipid tails are colored pink, cyan, black, and gray, respectively. (C) Top: DPPC gel phase at 329 K (heated from the gel phase at 250 K) and 319 K (cooled from the fluid phase at 350 K). Bottom: DPPC fluid phase at 331 K (heated from the gel at 250 K) and 321 K (cooled from the fluid phase at 350 K). Phosphatidyl and choline moieties and the glycerol linker are colored in pink, green, and black, respectively.

(Figure 6A). In the case of DLiPC-containing mixtures, the system separates into a gel−fluid coexistence, as experimentally expected.[38] This highlights the ability of cholesterol to disorder the DPPC gel phase into becoming fluid. At the same temperature, the DPPC/DOPC system without cholesterol becomes a homogeneous fluid phase. This is in contrast to the phase-separated cholesterol-containing system and shows the ability of cholesterol to induce phase separation even in fluid mixtures.

A modified cholesterol model, along the recommendation of Daily et al.,[40] was used to improve the behavior of cholesterol in lipid membranes. In particular, the protrusion of off-plane beads was increased by 60% compared with the original Martini model to prevent the overordering of L_o domains.[41] A similar strategy was recently also used to improve the cholesterol model in standard Martini.[42] Additionally, interactions between the polar bead of cholesterol and the charged lipid headgroup particles were specifically made more attractive in the dry model. The reason for this change is that the implicit model calls for increased repulsion between polar particle types to account for water screening; however, in the particular case of cholesterol−headgroup interactions, part of the screening is already done explicitly by the beads in the interfacial region, and their interaction therefore requires a less repulsive nature. This modification promotes the disordering effect of cholesterol by allowing it to sit at a shallow enough bilayer depth. The stronger headgroup interaction has the further benefit of preventing cholesterol from becoming too concentrated in the interleaflet plane (see Figure S5 in the Supporting Information).

As a more stringent test of the mixing behavior of lipids that differ in their lipid headgroup rather than tail, we compared binary systems composed of DOPC and DOPS (1:1). In the liquid-crystalline phase, these lipids are expected to mix well. Indeed, this is what we observe with both standard Martini and Dry Martini (Figure S6 in the Supporting Information). The final levels of mixing in the two models are almost indistinguishable.

One of the first successful applications of standard Martini was the transition from a multilamellar to an inverted hexagonal phase for dioleoylphosphatidylethanolamine (DOPE) lipids.[43] We repeated these simulations with Dry Martini. The system consists of two stacked DOPE bilayers with 256 lipids each, simulated at T = 350 K. To allow formation of the inverted hexagonal phase, an anisotropic pressure coupling was used together with nonzero off-diagonal components of the compressibility matrix, set to 3×10^{-5} bar^{-1}. However, we did not observe the expected transition to the inverted hexagonal phase in any of the 13 trial simulations of various length, totaling ~20 μs. A DOPE system in an inverted hexagonal configuration, on the other hand, was stable with Dry Martini, pointing to possible kinetic trapping of either phase in Dry Martini. The spontaneous transition between the lamellar and inverted hexagonal phases could be observed only with

long and highly unsaturated lipids, i.e., lipids with two or more unsaturations in both tails and lengths of at least five beads. An example of this transition is shown in Figure 6B. It should be noted that due to the absence of explicit solvent, the box volume shrinks during the transition. The water channels of the final (dry) inverted hexagonal phase are "filled" with the hydration shells of the lipid headgroups, which are implicitly included in the increased size of the Q-type particles.

The transition from a fluid to a gel-state membrane has also been successfully simulated in standard Martini.[44] To test whether the same transition can be observed in Dry Martini, we simulated a DPPC bilayer of 2048 lipids starting from a fluid phase (350 K) or a gel phase (250 K) and slowly cooling or heating, respectively, in steps of 2 K. Simulations at intermediate temperatures were 10 μs long to probe the phase behavior. A gel phase was obtained when the fluid phase was cooled below 321 K; starting from the gel phase, the system transitioned to a fluid phase at temperatures of 331 K and above. Snapshots of the gel and fluid bilayers obtained from either the heating or cooling cycle are shown in Figure 6C. Taking the transition temperature as the average of these two temperatures, we estimate the Dry Martini transition temperature of DPPC as 325 ± 5 K, which is somewhat higher than that of standard Martini (295 ± 5 K) but in fact closer to the experimental value for DPPC (314 K).[44] Notably, the shift in transition temperature is not the same for wet Martini and Dry Martini for all lipids. In the evaluation of general membrane properties, we found that for some lipids Dry Martini bilayers enter the gel phase whereas standard Martini bilayers remain fluid. The change in the transition temperature seems to be dependent on the lipid type. Especially, Dry Martini lipids with long, fully saturated tail lipids and PE or PC headgroups adopt a gel phase at lower temperature than with standard Martini. Interestingly, this behavior is also more in line with experimental observations.[38]

Another type of phase behavior that has been widely studied with standard Martini is micelle formation. The use of Dry Martini would offer a great computational benefit for these highly diluted systems. However, simulations of a number of systems comprising hundreds to thousands of surfactants, including lysoPC and negatively charged caprylic acid, reveal that although aggregates are formed, the individual aggregates have a strong tendency to cluster (see Figure S7 in Supporting Information). This is a direct consequence of the use of attractive pair potentials in Martini; the absence of explicit solvent allows the system to minimize its overall free energy by clustering of individual aggregates. Interestingly, an independent research group has found conditions under which micelles are in fact stable with Dry Martini by using particle mesh Ewald (PME) summation for electrostatic interactions (R. Larson, private communication). This avenue has not been further tested here.

As a final characterization of lipid phase behavior, we calculated the PMF of moving a lipid through the membrane to quantify how likely lipid flip-flops are and how difficult it is to extract a lipid from a membrane in wet Martini versus Dry Martini. A bilayer of 125 POPC lipids was used, with 62 lipids in each leaflet and one pulled through. The PMFs obtained with wet Martini and Dry Martini are shown in Figure 7. The two curves are very similar except for the lower free energy barrier in the center of the bilayer in Dry Martini. In each case, the barrier is large enough to prevent spontaneous flip-flops on submillisecond time scales, in line with the experimental

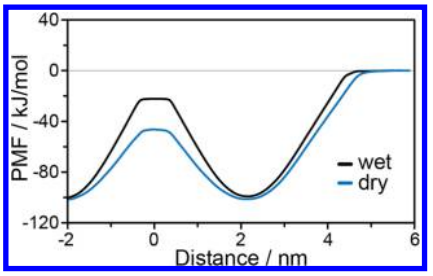

Figure 7. Free energy profiles for the processes of a POPC lipid flip-flop (distances from −2 to 2 nm) in and then extraction (distances from 2 to 5 nm) from a POPC bilayer. Profiles for both wet Martini and Dry Martini are reported. The center of the bilayer is at a distance of 0 nm.

evidence pointing to flip-flop rates of seconds to days for phospholipids.[45] Concerning the work required to extract a lipid from the membrane, it is quite remarkable that Dry Martini reproduces the free energy profile from membrane to water despite the total lack of interactions the lipid molecule experiences in the implicit-water phase.

3.6. Large-Scale Applications. Dry Martini offers a significant speedup in systems where water occupies a large proportion of the simulation box. Liposomes are prototypical examples of such systems. In standard Martini, the size of lipid vesicles is currently limited to 20−40 nm in diameter, and alternative approaches such as mean-field boundary potential to remove a significant amount of the water from both the inside and outside of the vesicle have been developed.[46] These sizes are the smallest range of vesicles that can be probed experimentally.

To study the properties of lipid vesicles modeled with Dry Martini, we first looked at the lamellar-to-vesicle transformation process. A pre-equilibrated POPC bilayer (361 lipids per leaflet) was placed at the center of a simulation box large enough that the bilayer patch was not connected to its own periodic image. The system was allowed to fully relax without any constraints under *NVT* conditions (Figure 8A). Lipid headgroups rapidly replaced the lipid tails exposed at the edges of the bilayer patch to form a bicellar intermediate (snapshot at t = 10 ns). A rather fast closure of the bicelle followed (t = 60, 70 ns) to form a small vesicle (t = 100 ns). This process of vesicle formation is identical to that described for standard Martini.[47]

We then explored vesicle fusion with Dry Martini. To reproduce previous simulation studies of this event with standard Martini,[48] two pre-equilibrated POPC vesicles (composed of 722 lipids each) were placed together with a minimum lipid−lipid separation of approximately 1 nm and simulated under *NVT* conditions. The sequence of events depicted in Figure 8B shows a rapid encounter of the vesicles potentially driven by the absence of explicit solvent, followed by the formation of a hemifused state (t = 10 ns). Subsequently, a fusion pore opens and connects the two inner leaflets, leading to an elongated vesicle (t = 20 ns), which slowly relaxes to a spherical shape (t = 2 μs). Apart from this last relaxation event, the stages of vesicle fusion observed in wet Martini and Dry Martini are similar.

Another application involving large proportions of solvent is the formation of tethers. A recent study described this process using standard Martini,[5] but at a large computational expense. We repeated some of these simulations using Dry Martini, removing the 90% of the system that was water, with a

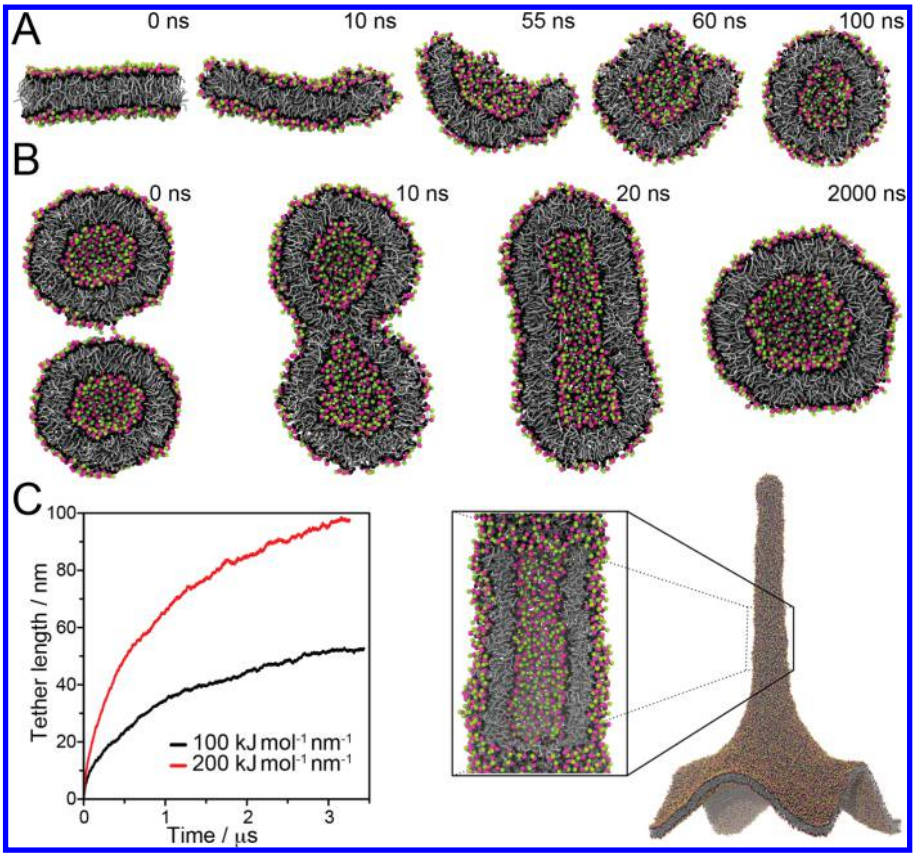

Figure 8. Prospective applications of Dry Martini. (A) Formation of a vesicle from a patch of pure POPC bilayer. Phosphatidyl and choline moieties, the glycerol linker, and the aliphatic section of the lipid tails are colored pink, green, black, and gray, respectively. To ease the visualization, the system was cut along a plane normal to the bilayer surface. (B) Fusion and stabilization of two DOPC vesicles into a larger one. Identical color-coding as in (A) is used, and the same system truncation was performed to show the fusion process. (C) Tether pulling of a system composed of modified DOPC lipids.[5] The tether length as a function of time is reported in the left panel for the two pulling forces tested. On the right, the conformation of the last frame of the 200 kJ mol^{-1} nm^{-1} simulation is shown using the same color-coding as in (A) and (B). The inset shows an incision of the tubular section of the tether demonstrating that it is hollow (i.e., filled with implicit water).

consequential drastic decrease in computational cost. Two membrane patches were simulated, a small one containing ∼4600 lipids and a large one with ∼22 000 lipids. We used the modified version of DOPC lipids derived by Baoukina et al.,[5] a model with more flexible tails. As for all of the other dry lipids, the bonds and angles were adjusted as detailed in section 3.1. Tethers were pulled from both small and large membrane patches using seven different pulling forces (10, 20, 50, 100, 150, 200, and 400 kJ mol^{-1} nm^{-1}) applied on a lipid patch with a radius of 3 nm. Details of the pulling setup can be found in the original publication.[5] In Figure 8C, the development of the tether for the large patch is shown for pulling forces of 100 and 200 kJ mol^{-1} nm^{-1} together with a snapshot at 1.3 μs of the same system pulled with the larger force. Similar to what Baoukina et al.[5] reported, it was found that a pulling force higher than 100 kJ mol^{-1} nm^{-1} is necessary for a tether to grow. Forces lower than 100 kJ mol^{-1} nm^{-1} did not result in tether formation but instead resulted in protrusions and bending of the bilayer. Linear elongation of the tube was also limited by the finite bilayer size in the simulation. As with standard Martini, the tether formation was reversible: reduction or removal of the external force resulted in tether retraction or complete membrane respreading. Thus, our results utilizing the Dry Martini force field correlate very well with those reported by Baoukina et al.[5] It is worth mentioning that this type of simulation did not lead to tether formation when carried out with standard Martini DOPC lipids. The need for extra-flexible lipid tails seems to be crucial for the formation of tethers, at least on the time scale accessible to our simulations.

3.7. Proteins. In this section we describe some tests on the combination of the Dry Martini lipid model with proteins. Differences may be expected because of the changes in the interaction matrix. We first analyzed the behavior of single amino acid side chains by computing side chain−side chain PMFs in various solvents for which reference simulations are available for standard Martini.[49] PMFs were determined for every possible side-chain pair in both dry "water" and hexadecane. Results for three pairs are presented in Figure 9, and the complete set of PMFs is available upon request. The general trend is as follows: PMFs for side chains consisting of a single bead (Asn, Cys, Gln, Leu, etc.) reproduce standard Martini values relatively well, in line with the results shown in section 3.2. However, as soon as the complexity of the side chain increases, the lack of an entropy contribution from the solvent becomes problematic, causing an overestimation of the dimer stability in the aqueous phase and an underestimation in apolar solvents. We also determined the partitioning free energies of each side-chain analogue between the same five solvents used for the single beads in section 3.3. The results and their comparison to standard Martini are presented in Table S3 in the Supporting Information. Dry Martini reproduces reasonably well the partitioning of side-chain analogues

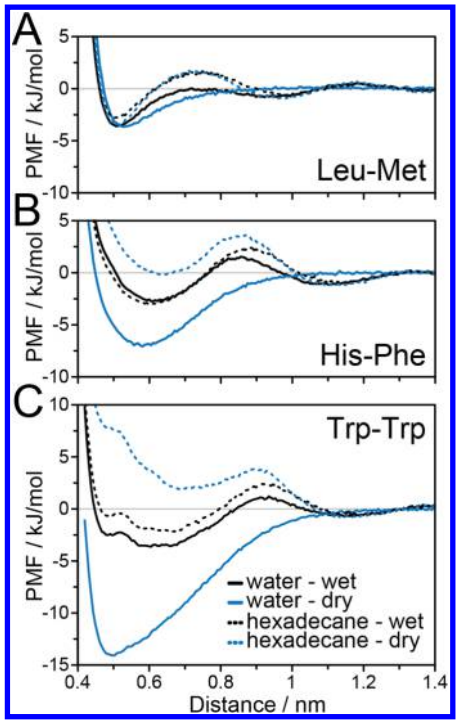

Figure 9. Side chain−side chain PMFs in both aqueous and apolar solvents. Three types of interactions involving side chains of different sizes are reported: (A) leucine−methionine pair, (B) histidine−phenylalanine pair, and (C) tryptophan−tryptophan pair.

consisting of a single bead, but again the correspondence gets increasingly worse with increasing complexity of the side chain. Partitioning free energies for the aromatic side chains do not match the reference values of the standard model.

To test the effect of these discrepancies on a simple membrane protein, we performed a simulation of a transmembrane helix, KALP,[50,51] embedded in either a wet Martini or Dry Martini DPPC bilayer. The system consisted of 316 DPPC lipids and four copies of KALP and was simulated for 1 μs at T = 330 K. A snapshot of the dry simulation is shown in Figure 10A. In both wet Martini and Dry Martini, the formation of dimers is observed. We also note very similar tilting modes for the isolated helices and comparable dynamics of the lysine residues located on each extremity of the peptides. To further characterize the behavior of KALP helices in a bilayer, PMFs for dimerization were computed for both models using the umbrella sampling technique as described in Methods. The resulting PMFs (Figure 10B) have similar shapes and predict a stable dimeric state, but the level of attraction between the peptides is much reduced with Dry Martini.

4. DISCUSSION

We have presented a new flavor of the Martini CG model: the Dry Martini version, which omits the aqueous phase. We parametrized Dry Martini to reproduce the main features of the standard (or wet) version, focusing on lipid systems. We chose not to include an explicit solvation term in the model but rather to adjust the nonbonded interaction matrix of standard Martini. Removing the solvent allows for a considerable reduction in computational cost, but the lack of solvent in simulation boxes induces a few limitations. The adjustment of the nonbonded interactions to implicitly include the effect of water led to the need for recalibration of some bonded interactions as well. The

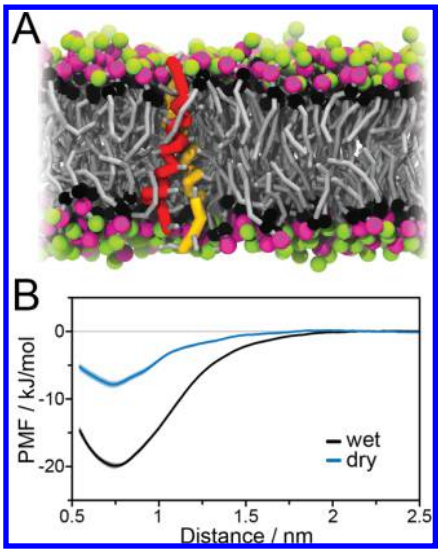

Figure 10. Illustration of the use of Dry Martini for membrane proteins. (A) Snapshot of KALP helices (red/yellow) embedded in a DPPC bilayer simulated with Dry Martini. Phosphatidyl and choline moieties, the glycerol linker, and the aliphatic section of the lipid tails of the DPPC membrane are colored in pink, green, black, and gray, respectively. (B) PMFs as functions of distance between the centers of mass of the KALP peptides.

decrease in the number of degrees of freedom conceptually makes the force field even "coarser". Therefore, the water-free model is more qualitative in nature, although properties of membranes are relatively well preserved between wet Martini and Dry Martini. Importantly, Dry Martini keeps the flexibility and simplicity of the Martini building block approach, allowing easy extension of the model to other (bio)molecular systems. Together with the drastic speedup and the possibility to simulate order-of-magnitude larger systems, we expect the Dry Martini model to become a useful alternative to existing water-free models. Below we discuss the limitations, benefits, and potential applications of Dry Martini in more detail.

4.1. Limitations of the Model. A significant limitation of CG force fields in general is due to the reduction of the entropy contribution in the simulated systems. In Martini some degrees of freedom are removed to convert chemical groups into beads, and the total entropy of the system is not conserved.[52] This issue is usually alleviated by counterbalancing the missing entropy with enthalpic components. Dry Martini is not an exception, as additional degrees of freedom have been removed compared with the standard Martini version, and it is necessary to account for the missing entropy of the system (here water degrees of freedom). To do so, the LJ interactions between apolar beads have been increased, providing a driving force mimicking the hydrophobic effect. On the other hand, the strength of LJ interactions involving polar and charged particles has been decreased to take into account the implicit screening effect of hydrating water molecules.

These modifications bring about some important limitations, e.g., simulations of systems involving mainly polar interactions are not reliable with Dry Martini. Highly polar solvents have weak interactions in Dry Martini and thus prefer the gas phase at room temperature. Dry Martini is meant for simulations where water is the main solvent and where the implicit description of water can offer a large speedup relative to standard Martini. In all other systems, standard Martini should

be used. It should be emphasized that in Dry Martini, a bead modeled to be in vacuum is actually in the (implicit) liquid water phase. This also means that by definition there is no gas phase in Dry Martini. A traditional system of a solvent in a condensed phase coexisting with its gas phase describes a two-phase system. In Dry Martini, particles that escape the condensed phase to go into the gas phase in fact enter the implicit liquid water phase. The related consequence is the impossibility to simulate systems solvated in polar solvents other than water.

Another limitation of Dry Martini arises from the absence of purely repulsive interaction potentials (except between like-charge particles). As the nonbonded interactions are modeled using LJ potentials, all of the pair interactions are attractive. In the current version, this prevents, for instance, the simulation of soluble proteins or equilibrium between membrane-bound and dissolved populations of compounds (drugs, amphiphiles, etc.). The inability to simulate the dynamics of micellar solutions (cf. Figure S7 in the Supporting Information) is another example. Simulations of such systems will in general lead to global aggregation of the molecules or aggregates present in the simulation cell. This is not a fundamental problem of implicit-solvent models, however, and is certainly due to our choice of using LJ potentials to model the nonbonded interactions. A straightforward way to improve the model in this respect would be to add tabulated potentials. Such potentials can be derived from appropriate AA reference simulations, as has been shown by others.[14,15]

A few words of concern should also be directed toward the use of ions in Dry Martini. Most implicit-solvent models integrate out the ionic degrees of freedom, representing the ionic strength with a mean-field term. We decided to treat ions explicitly for three reasons: (i) explicit ions provide some screening of the electrostatic interactions, making it possible to capture (qualitatively) ionic strength effects and treat inhomogeneous systems; (ii) explicit ions provide the necessary counterions to compensate charges present elsewhere in the system; and (iii) implicit-solvent ionic solutions were used to parametrize the ionic interactions occurring in the lipid headgroup region. It is important to stress, however, that the use of ions in Dry Martini, and also in standard Martini, should be considered with care.

The lack of water also causes an unwanted stabilization of compounds formed of tightly packed beads, i.e., CG molecules in which beads partially overlap, such as aromatic rings. This artifact is due to the way the implicit presence of water has been parametrized in the model: the free energy term due to formation of a cavity in water has been included in the interactions of the single beads with other solvents, and especially with nonpolar beads. This approach assumes that the cavity term will increase linearly with particle number for larger molecules. However, many of the protein side chains in Martini are formed of closely packed beads that require a cavity of significantly different size from the sum of cavities required by each of the beads individually. This leads to difficulties in balancing the missing cavity formation term with other interactions present in the system. Consequently, partitioning and dimerization free energies for compact molecules are not properly reproduced with the current version of Dry Martini (cf. Figure 9 and Table S3 in the Supporting Information). As an example of the consequence of this effect in a biological system, we showed the aggregation propensity of KALP peptides to be underestimated (Figure 10B). Even though this might actually be an advantage in terms of sampling, applications of this kind should be considered rather qualitatively.

4.2. Speedup. The main advantage of Dry Martini is obviously the decreased computational cost. The gain will naturally be proportional to the number of water beads removed. In a simple bilayer system, where about half the system is composed of lipids, the improvement will be less significant than for a system composed of a large vesicle ($\sim 10^4$ lipids) where >90% of the simulation box is filled with water ($\sim 10^6$ particles). Within this study, we found speedups ranging from close to a factor of 2 for small bilayer systems to 1−2 orders of magnitude for a vesicle with a diameter of ∼100 nm. This speedup is only computational; other effects need to be taken into account, such as the kinetics of the processes studied. As mentioned already, the introduction of friction into the equations of motion (through the use of the SD integrator) results in a decrease in lipid diffusion compared with standard Martini. A more complete scan of the effect of the coupling time constant τ_T, dictating the amount of friction applied to the system, was used to quantify the effect on lipid diffusion. The results are presented in Table S1 in the Supporting Information. A value of τ_T in the range 1−10 ps appears to be the best compromise between not posing too much friction on the one hand while maintaining effective temperature control on the other. In the current work, we used τ_T = 4 ps. It should be noted that much better temperature control is observed with the recently developed new SD integrator by Goga et al.[53] In fact, at least for the bilayer simulations tested here, a standard MD integrator can also be used, together with a weak temperature coupling scheme. Even in this case, the lipid diffusion rates of Dry Martini are still a factor of 2 lower than those of standard Martini. We attribute this remaining difference to the increased strength of the nonbonded interactions between the lipid tails in Dry Martini, mimicking the hydrophobic effect.

Besides the computational advantage due to a reduced number of particles, a few other issues are also important in assessing the efficiency of Dry Martini. In the highly inhomogeneous example of a large vesicle, the algorithm used (in GROMACS) to split the force calculations over multiple processors is also of prime importance. With most of the system now being vacuum (implicit water), the domain decomposition for parallel computation needs to be chosen with care. Finally, some applications may benefit from the increased sampling rate due to the decrease or absence of energetic barriers. In particular, hydration barriers do not exist in Dry Martini, causing, e.g., fast membrane fusion (cf. Figure 6B).

4.3. Applications. The Dry Martini force field has been primarily designed for simulations of systems containing a large amount of aqueous solvent. In its current form, aimed at reproducing lipid properties, applications involving membrane remodeling seem most appropriate; with Dry Martini, the macroscopic limit is within reach. The fact that Dry Martini inherits all of the lipid topologies from the standard model implies that the behavior of multicomponent membranes can be readily explored. For instance, the role of membrane domains such as lipid rafts on membrane fusion and fission can be studied over a large range of system sizes, and state conditions can be systematically probed.

Another range of applications of Dry Martini is for equilibration purposes. Because of the reduction in particle

numbers and the absence of hydration barriers, we found Dry Martini to reach equilibrium states with much less computational effort compared with the standard version. An effective strategy for setting up a new system would be to equilibrate it first with Dry Martini, after which the system would be solvated and continued using standard Martini. The lipid bead types are identical in the two models, and only some adjustment of bonded interactions is required. For lipids that are not part of the large set of common lipids presented here, that would require some additional effort, using either existing Martini topologies or atomistic simulations as a reference.

Given the similarity between the wet Martini and Dry Martini models, the simultaneous use of both wet and dry models within the same system could be drafted, allowing "finer" descriptions of the interactions where needed. As a proof of principle, we simulated a water-filled vesicle with the outer membrane described with Dry Martini and the inner membrane with standard Martini (Figure 11). Cross interactions were treated as in standard Martini.

5. CONCLUSIONS

We have provided a water-free version of the popular Martini CG force field based on a careful recalibration of the pairwise interaction matrix of the building blocks (the CG beads). The new model, called Dry Martini, performs well in describing general membrane properties. Area per lipid, membrane thickness, area compressibility, and lipid order compare well to those of standard Martini for a large set of different lipids. Collective processes such as domain formation and gel-phase transition are also reproduced in Dry Martini. However, the model has limitations. In its current form, the model does not mimic aqueous solutions very well. Notably, protein interactions in the aqueous phase are not modeled realistically. Applications involving membrane proteins have to be considered with care, and more systematic testing of peptide/lipid systems still has to be performed. Keeping these restrictions in mind, the potential of the Dry Martini model is wide. The model benefits from the extensive set of existing well-studied systems of standard Martini. We expect Dry Martini to be particularly useful in the study of membrane processes involving 10^5–10^7 lipids, including, for example, liposome fusion and budding, tether formation, lateral domain formation, and large-scale membrane dynamics organization.

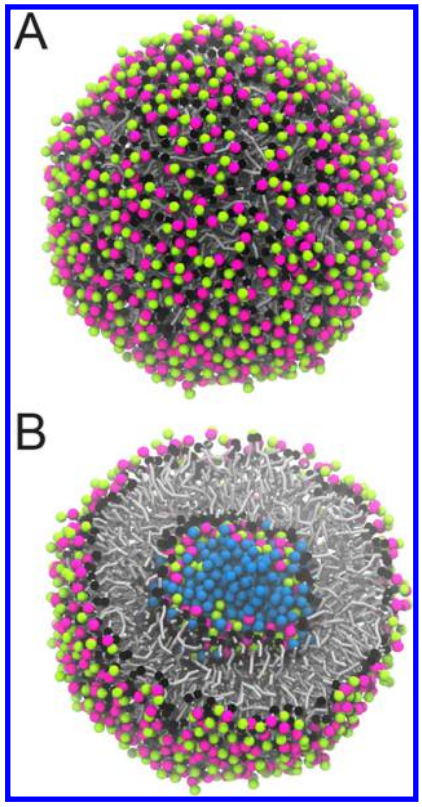

Figure 11. Snapshots of a water-filled vesicle simulated using a combination of the wet Martini and Dry Martini force fields. The lipids in the inner leaflet and the encapsulated water (blue spheres) were described using the standard Martini parameters. In the outer leaflet the Dry Martini parameters were used. Standard Martini nonbonded parameters were used to describe cross interactions. The conformation reported here corresponds to the final structure obtained after a 1 μs simulation, viewed from the outside in (A) and sliced in the middle in (B).

■ ASSOCIATED CONTENT

Ⓢ Supporting Information

Tables with diffusion coefficient vs friction time constant, lipid properties, and partition free energies of residue side chains (Tables S1–S3, respectively); comparison of wet Martini and Dry Martini interaction matrices, bonded parameter distributions, lipid property correlation plots, undulation spectra, cholesterol distribution, micelle aggregation, and lateral mixing (Figures S1–S7). This material is available free of charge via the Internet at http://pubs.acs.org.

■ AUTHOR INFORMATION

Corresponding Author

*E-mail: s.j.marrink@rug.nl. Fax: + 31-50-3634398. Tel: + 31-50-3634457.

Author Contributions

†C.A. and J.J.U. contributed equally. C.A. and J.J.U. wrote the paper; C.A., J.J.U., M.F.M., H.I.I., D.H.d.J., M.N.M., and X.P. performed the simulations and the analysis; and X.P., A.H.d.V., and S.J.M. interpreted the data and designed the research.

Funding

J.J.U. was supported by a Ph.D. scholarship from the Emil Aaltonen Foundation. H.I.I. was supported by a Rubicon Grant from The Netherlands Organization for Scientific Research (NWO). Computational resources from NWO at SARA are acknowledged.

Notes

The authors declare no competing financial interest.

■ REFERENCES

(1) Noid, W. G. Perspective: Coarse-Grained Models for Biomolecular Systems. *J. Chem. Phys.* **2013**, *139*, No. 090901.

(2) Ingólfsson, H. I.; López, C. A.; Uusitalo, J. J.; de Jong, D. H.; Gopal, S. M.; Periole, X.; Marrink, S.-J. The Power of Coarse Graining in Biomolecular Simulations. *Wiley Interdiscip. Rev.: Comput. Mol. Sci.* **2013**, *4*, 225–248.

(3) Marrink, S.-J.; Tieleman, D. P. Perspective on the Martini Model. *Chem. Soc. Rev.* **2013**, *42*, 6801–6822.

(4) Kleinjung, J.; Fraternali, F. Design and Application of Implicit Solvent Models in Biomolecular Simulations. *Curr. Opin. Struct. Biol.* **2014**, *25*, 126–134.

(5) Baoukina, S.; Marrink, S.-J.; Tieleman, D. P. Molecular Structure of Membrane Tethers. *Biophys. J.* **2012**, *102*, 1866–1871.

(6) Yesylevskyy, S. O.; Schäfer, L. V.; Sengupta, D.; Marrink, S.-J. Polarizable Water Model for the Coarse-Grained MARTINI Force Field. *PLOS Comput. Biol.* **2010**, *6*, No. e1000810.
(7) Wu, Z.; Cui, Q.; Yethiraj, A. A New Coarse-Grained Model for Water: The Importance of Electrostatic Interactions. *J. Phys. Chem. B* **2010**, *114*, 10524−10529.
(8) Noguchi, H. Membrane Simulation Models from Nanometer to Micrometer Scale. *J. Phys. Soc. Jpn.* **2009**, *78*, No. 041007.
(9) Murtola, T.; Bunker, A.; Vattulainen, I.; Deserno, M.; Karttunen, M. Multiscale Modeling of Emergent Materials: Biological and Soft Matter. *Phys. Chem. Chem. Phys.* **2009**, *11*, 1869−1892.
(10) Lyubartsev, A. P.; Rabinovich, A. L. Recent Development in Computer Simulations of Lipid Bilayers. *Soft Matter* **2010**, *7*, 25−39.
(11) West, B.; Brown, F. L. H.; Schmid, F. Membrane−Protein Interactions in a Generic Coarse-Grained Model for Lipid Bilayers. *Biophys. J.* **2009**, *96*, 101−115.
(12) Sevink, A.; Fraaije, J. Efficient Solvent-Free Dissipative Particle Dynamics for Lipid Bilayers. *Soft Matter* **2014**, *10*, 5129−5146.
(13) Izvekov, S.; Voth, G. A. Solvent-Free Lipid Bilayer Model Using Multiscale Coarse-Graining. *J. Phys. Chem. B* **2009**, *113*, 4443−4455.
(14) Lu, L.; Voth, G. A. Systematic Coarse-Graining of a Multicomponent Lipid Bilayer. *J. Phys. Chem. B* **2009**, *113*, 1501−1510.
(15) Lyubartsev, A. P.; Mirzoev, A.; Chen, L.; Laaksonen, A. Systematic Coarse-Graining of Molecular Models by the Newton Inversion Method. *Faraday Discuss.* **2009**, *144*, 43−56.
(16) Wang, Z.-J.; Deserno, M. A Systematically Coarse-Grained Solvent-Free Model for Quantitative Phospholipid Bilayer Simulations. *J. Phys. Chem. B* **2010**, *114*, 11207−11220.
(17) Cooke, I. R.; Kremer, K.; Deserno, M. Tunable Generic Model for Fluid Bilayer Membranes. *Phys. Rev. E* **2005**, *72*, No. 011506.
(18) Sodt, A. J.; Head-Gordon, T. An Implicit Solvent Coarse-Grained Lipid Model with Correct Stress Profile. *J. Chem. Phys.* **2010**, *132*, No. 205103.
(19) Curtis, E. M.; Hall, C. K. Molecular Dynamics Simulations of DPPC Bilayers Using "LIME," a New Coarse-Grained Model. *J. Phys. Chem. B* **2013**, *117*, 5019−5030.
(20) Srivastava, A.; Voth, G. A. Hybrid Approach for Highly Coarse-Grained Lipid Bilayer Models. *J. Chem. Theory Comput.* **2013**, *9*, 750−765.
(21) Pronk, S.; Páll, S.; Schulz, R.; Larsson, P.; Bjelkmar, P.; Apostolov, R.; Shirts, M. R.; Smith, J. C.; Kasson, P. M.; van der Spoel, D.; Hess, B.; Lindahl, E. GROMACS 4.5: A High-Throughput and Highly Parallel Open Source Molecular Simulation Toolkit. *Bioinformatics* **2013**, *29*, 845−854.
(22) Bussi, G.; Donadio, D.; Parrinello, M. Canonical Sampling through Velocity Rescaling. *J. Chem. Phys.* **2007**, *126*, No. 014101.
(23) Berendsen, H. J. C.; Postma, J. P. M.; van Gunsteren, W. F.; DiNola, A.; Haak, J. R. Molecular Dynamics with Coupling to an External Bath. *J. Chem. Phys.* **1984**, *81*, 3684−3690.
(24) Parrinello, M. Polymorphic Transitions in Single Crystals: A New Molecular Dynamics Method. *J. Appl. Phys.* **1981**, *52*, 7182−7190.
(25) Marrink, S.-J.; Periole, X.; Tieleman, D. P.; de Vries, A. H. Comment on "On Using a Too Large Integration Time Step in Molecular Dynamics Simulations of Coarse-Grained Molecular Models" by M. Winger, D. Trzesniak, R. Baron and W. F. Van Gunsteren. *Phys. Chem. Chem. Phys.* **2009**, *11*, 1934; *Phys. Chem. Chem. Phys.* **2010**, *12*, 2254−2258.
(26) Bennett, C. H. Efficient Estimation of Free Energy Differences from Monte Carlo Data. *J. Comput. Phys.* **1976**, *22*, 245−268.
(27) Torrie, G.; Torrie, G.; Valleau, J.; Valleau, J. Nonphysical Sampling Distributions in Monte Carlo Free-Energy Estimation: Umbrella Sampling. *J. Comput. Phys.* **1977**, *23*, 187−199.
(28) Kumar, S.; Rosenberg, J. M.; Bouzida, D.; Swendsen, R. H.; Kollman, P. A. The Weighted Histogram Analysis Method for Free-Energy Calculations on Biomolecules. I. The Method. *J. Comput. Chem.* **1992**, *13*, 1011−1021.
(29) Hub, J. S.; de Groot, B. L.; van der Spoel, D. G_WHAM—A Free Weighted Histogram Analysis Implementation Including Robust Error and Autocorrelation Estimates. *J. Chem. Theory Comput.* **2010**, *6*, 3713−3720.
(30) Marrink, S.-J.; de Vries, A. H.; Mark, A. E. Coarse Grained Model for Semiquantitative Lipid Simulations. *J. Phys. Chem. B* **2004**, *108*, 750−760.
(31) Ollila, S.; Risselada, H. J.; Louhivuori, M.; Lindahl, E.; Vattulainen, I.; Marrink, S.-J. 3D Pressure Field in Lipid Membranes and Membrane−Protein Complexes. *Phys. Rev. Lett.* **2009**, *102*, No. 078101.
(32) Brandt, E. G.; Braun, A. R.; Sachs, J. N.; Nagle, J. F.; Edholm, O. Interpretation of Fluctuation Spectra in Lipid Bilayer Simulations. *Biophys. J.* **2011**, *100*, 2104−2111.
(33) Marrink, S.-J.; Risselada, H. J.; Yefimov, S.; Tieleman, D. P.; de Vries, A. H. The MARTINI Force Field: Coarse Grained Model for Biomolecular Simulations. *J. Phys. Chem. B* **2007**, *111*, 7812−7824.
(34) Marrink, S.-J.; Lindahl, E.; Edholm, O. Simulation of the Spontaneous Aggregation of Phospholipids into Bilayers. *J. Am. Chem. Soc.* **2001**, *123*, 8638−8639.
(35) Ollila, S.; Hyvönen, M. T.; Vattulainen, I. Polyunsaturation in Lipid Membranes: Dynamic Properties and Lateral Pressure Profiles. *J. Phys. Chem. B* **2007**, *111*, 3139−3150.
(36) Hu, M.; de Jong, D. H.; Marrink, S.-J.; Deserno, M. Gaussian Curvature Elasticity Determined from Global Shape Transformations and Local Stress Distributions: A Comparative Study Using the MARTINI Model. *Faraday Discuss.* **2013**, *161*, 365−382.
(37) Marsh, D. Elastic Curvature Constants of Lipid Monolayers and Bilayers. *Chem. Phys. Lipids* **2006**, *144*, 146−159.
(38) Marsh, D. *Handbook of Lipid Bilayers*; CRC Press: Boca Raton, FL, 2013.
(39) Risselada, H. J.; Marrink, S.-J. The Molecular Face of Lipid Rafts in Model Membranes. *Proc. Natl. Acad. Sci. U.S.A.* **2008**, *105*, 17367−17372.
(40) Daily, M. D.; Olsen, B. N.; Schlesinger, P. H.; Ory, D. S.; Baker, N. A. Improved Coarse-Grained Modeling of Cholesterol Activation in Lipid Bilayers. *Biophys. J.* **2013**, *104*, 590A−591A.
(41) Duncan, S. L.; Dalal, I. S.; Larson, R. G. Molecular Dynamics Simulation of Phase Transitions in Model Lung Surfactant Monolayers. *Biochim. Biophys. Acta* **2011**, *1808*, 2450−2465.
(42) Ingólfsson, H. I.; Melo, M. N.; van Eerden, F. J.; Arnarez, C.; López, C. A.; Wassenaar, T. A.; Periole, X.; de Vries, A. H.; Tieleman, D. P.; Marrink, S.-J. Lipid Organization of the Plasma Membrane. *J. Am. Chem. Soc.* **2014**, *136*, 14554−14559.
(43) Marrink, S.-J.; Mark, A. E. Molecular View of Hexagonal Phase Formation in Phospholipid Membranes. *Biophys. J.* **2004**, *87*, 3894−3900.
(44) Marrink, S.-J.; Risselada, H. J.; Mark, A. E. Simulation of Gel Phase Formation and Melting in Lipid Bilayers Using a Coarse Grained Model. *Chem. Phys. Lipids* **2005**.
(45) Menon, A. K. Flippases. *Trends Cell Biol.* **1995**, *5*, 355−360.
(46) Risselada, H. J.; Mark, A. E.; Marrink, S.-J. Application of Mean Field Boundary Potentials in Simulations of Lipid Vesicles. *J. Phys. Chem. B* **2008**, *112*, 7438−7447.
(47) Marrink, S.-J.; Mark, A. E. Molecular Dynamics Simulation of the Formation, Structure, and Dynamics of Small Phospholipid Vesicles. *J. Am. Chem. Soc.* **2003**, *125*, 15233−15242.
(48) Marrink, S.-J.; Mark, A. E. The Mechanism of Vesicle Fusion As Revealed by Molecular Dynamics Simulations. *J. Am. Chem. Soc.* **2003**, *125*, 11144−11145.
(49) de Jong, D. H.; Periole, X.; Marrink, S.-J. Dimerization of Amino Acid Side Chains: Lessons from the Comparison of Different Force Fields. *J. Chem. Theory Comput.* **2012**, *8*, 1003−1014.
(50) de Planque, M. R. R.; Kruijtzer, J. A. W.; Liskamp, R. M. J.; Marsh, D.; Greathouse, D. V.; Koeppe, R. E.; de Kruijff, B.; Killian, J. A. Different Membrane Anchoring Positions of Tryptophan and Lysine in Synthetic Transmembrane α-Helical Peptides. *J. Biol. Chem.* **1999**, *274*, 20839−20846.

(51) Killian, J. A. Synthetic Peptides as Models for Intrinsic Membrane Proteins. *FEBS Lett.* **2003**, *555*, 134−138.
(52) Baron, R.; Trzesniak, D.; de Vries, A. H.; Elsener, A. Comparison of Thermodynamic Properties of Coarse-Grained and Atomic-Level Simulation Models. *Chem. Phys. Phys. Chem.* **2007**, *8*, 452−461.
(53) Goga, N.; Rzepiela, A. J.; de Vries, A. H.; Marrink, S.-J.; Berendsen, H. J. C. Efficient Algorithms for Langevin and DPD Dynamics. *J. Chem. Theory Comput.* **2012**, *8*, 3637−3649.
(54) *CRC Handbook of Chemistry and Physics*; Lide, D. R., Ed.; CRC Press: Boca Raton, FL, 1993.
(55) Duffy, E. M.; Jorgensen, W. L. Prediction of Properties from Simulations: Free Energies of Solvation in Hexadecane, Octanol, and Water. *J. Am. Chem. Soc.* **2000**, *122*, 2878−2888.
(56) Wolfenden, R.; Andersson, L.; Cullis, P. M.; Southgate, C. C. B. Affinities of Amino Acid Side Chains for Solvent Water. *Biochemistry* **1981**, *20*, 849−855.
(57) Ruelle, P. The *n*-Octanol and *n*-Hexane/Water Partition Coefficient of Environmentally Relevant Chemicals Predicted from the Mobile Order and Disorder (MOD) Thermodynamics. *Chemosphere* **2000**, *40*, 457−512.
(58) Dolney, D. M.; Hawkins, G. D.; Winget, P.; Liotard, D. A.; Cramer, C. J.; Truhlar, D. G. Universal Solvation Model Based on Conductor-Like Screening Model. *J. Comput. Chem.* **2000**, *21*, 340−366.
(59) Abraham, M. H.; Whiting, G. S.; Fuchs, R.; Chambers, E. J. Thermodynamics of Solute Transfer from Water to Hexadecane. *J. Chem. Soc., Perkin Trans. 2* **1990**, 291−300.
(60) Hansch, C.; Leo, A.; Hoekman, D.; Heller, S. R. *Exploring QSAR—Hydrophobic, Electronic, and Steric Constants*; American Chemical Society: Washington, DC, 1995.
(61) Rand, R. P.; Parsegian, V. A. Hydration Forces between Phospholipid Bilayers. *Biochim. Biophys. Acta* **1989**, *988*, 351−376.
(62) Pabst, G.; Rappolt, M.; Amenitsch, H.; Laggner, P. Structural Information from Multilamellar Liposomes at Full Hydration: Full Q-Range Fitting with High Quality X-Ray Data. *Phys. Rev. E* **2000**, *62*, 4000−4009.
(63) Kucerka, N.; Tristram-Nagle, S.; Nagle, J. F. Structure of Fully Hydrated Fluid Phase Lipid Bilayers with Monounsaturated Chains. *J. Membr. Biol.* **2005**, *208*, 193−202.
(64) Kucerka, N.; Nieh, M.-P.; Katsaras, J. Fluid Phase Lipid Areas and Bilayer Thicknesses of Commonly Used Phosphatidylcholines as a Function of Temperature. *Biochim. Biophys. Acta* **2011**, *1808*, 2761−2771.
(65) Binder, H.; Gawrisch, K. Dehydration Induces Lateral Expansion of Polyunsaturated 18:0-22:6 Phosphatidylcholine in a New Lamellar Phase. *Biophys. J.* **2001**, *81*, 969−982.
(66) Gaede, H. C.; Gawrisch, K. Lateral Diffusion Rates of Lipid, Water, and a Hydrophobic Drug in a Multilamellar Liposome. *Biophys. J.* **2003**, *85*, 1734−1740.